Supplementary Information
A synchronized quorum of genetic clocks

Tal Danino[1,⋆], Octavio Mondragón-Palomino[1,⋆], Lev Tsimring[2], & Jeff Hasty[1,2,3,4]

November 2, 2009

[1] *Department of Bioengineering, University of California, San Diego, San Diego, California, USA.*
[2] *BioCircuits Institute, University of California, San Diego, San Diego, California, USA.*
[3] *Molecular Biology Section, Division of Biological Science, University of California, San Diego, La Jolla, CA 92093, USA*
[4] *Corresponding Author. Molecular Biology Section, Division of Biological Science, University of California, San Diego, Mailcode 0412, La Jolla, CA 92093-0412, USA. Telephone: 858 822 3442. Fax: 858 534 5722. Email: hasty@ucsd.edu*

⋆ These authors contributed equally to this work.

Plasmid Construction

The pTD103 plasmids were constructed by replacing the promoter in a pZ modular plasmid (pZE21yemGFP-LAA) from XhoI to EcoRI restriction sites(Lutz and Bujard (1997)) with the *luxR* gene and the *luxI* promoter amplified via PCR from the native *Vibrio Fischeri* operon(pJE202, Dunlap and Greenberg (1985)). The pZ plasmid RBS was kept the same, and *luxI* or *aiiA*(from pMAL-t-aiiA, Thomas et al. (2005)) genes were cloned in place of yemGFP with the TSAANDENYALAA degradation tag on the carboxy-terminal(Stricker et al. (2008)). The yemGFP reporter module (luxR gene-luxIp-yemGFP-LAA) was then amplified with AvrII and NheI restriction sites and ligated into the AvrII site following the terminator in pTD103luxI-LAA.

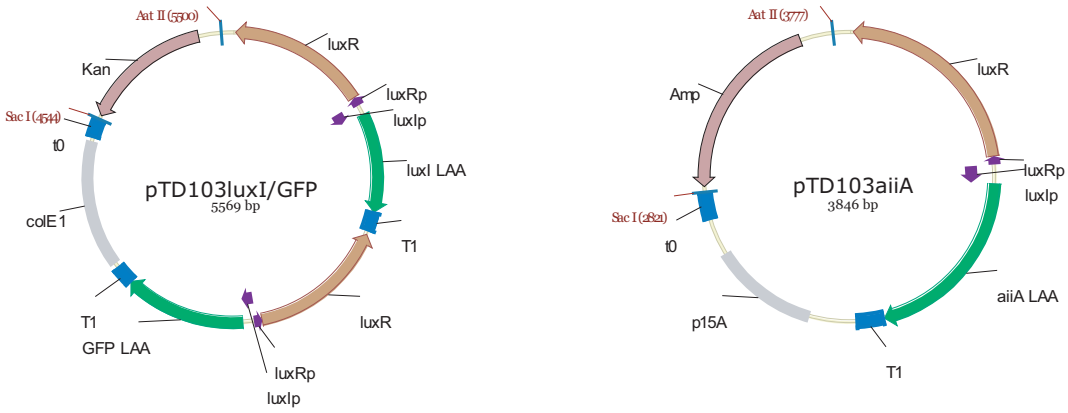

Supplementary Figure 1: Plasmids for the synchronized oscillator strain TDQS1. Construction of the pTD103 plasmids was done in the modular pZ plasmid backbones in three identical transcriptional modules with the same promoter, RBS, and terminator for each.

Data Analysis

Fluorescence vs. Time curves were obtained by importing fluorescent images into ImageJ and using the 'Intensity vs. Time Monitor' Plug-in to obtain a mean gray value of the entire field of view, and then the background gray value was subtracted (Fig1c 60x magnification, Fig 2a,b 20x magnification). Peak-to-peak values were taken for all period measurements and amplitudes were measured as peak to previous trough values. The data collected in Fig2c,d was obtained from 20x/60x magnification experiments from the parallelized device (Supplement Fig. 3b) in different sized traps. Each data point in Fig. 2c,d represents between 10-40 peak values averaged. We found that traps downstream of each other had similar period/amplitude measurements and including them in our averages did not significantly alter the mean values but greatly reduced the errors bar values. This showed that traps downstream of one another were only weakly coupled at our flow rates. In Suppl Fig2, we plot an additional fluorescence trajectory obtained from imaging one of these traps at 60x showing that oscillations exhibit stably over long periods of time.

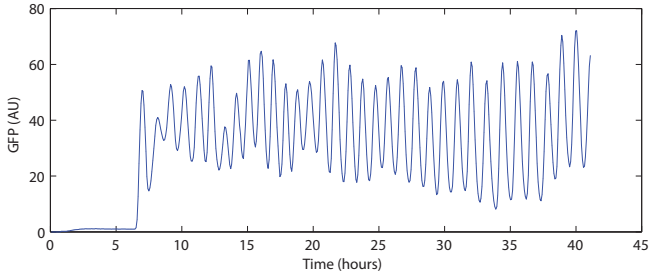

Supplementary Figure 2: *Stable oscillations in microfluidic device.* Fluorescence vs. Time curve obtained for a 100x84 micron trap over the course of $\sim$ 40 hours.

Space-Time plots

To create the space-time plot in Fig 3b, we averaged a 20 pixel window along the center of the trap (seen in Fig3a) in fluorescent images. To obtain a semi-quantitative measure of cell density we performed the same process on brightfield images. When no cells were present, the mean gray value was darker due to the lighting on the PDMS (polydimethylsiloxane) device, so we manually corrected the blue region in the bottom left of Suppl. Fig3 where no cells were present. Once cells populated the trap, we found the gray value to give a measure of the density cells (Suppl. Fig3). The periodicity in the data (apparent at high time values) is an artifact from the stitching of images in the Nikon Elements software (due to the slight difference in focal planes when the camera moves). We obtained the space time plot for Fig3d by averaging the fluorescence (20 pixel window) along the center of the colony. We stitched together 3 continuous image sets with image frequencies of 4 minutes (1-45), 3 minutes (frames 46-99) and 2.25 minutes (frames greater than 100). In the displayed images, another colony growing from bottom left begins to merge with the main one, and slightly influences the fluorescent front on the left but did not affect the front to the right.

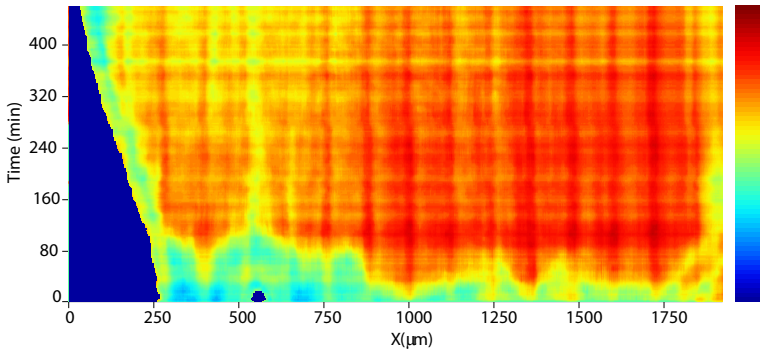

Supplementary Figure 3: *Space-time plot of density of cells in Fig3a experiment.* Gray value of the brightfield images is plotted as a measure of cell density in the 2000x100x0.95μm device. Red indicates higher cell density.

Microscopy and Microfluidics

A similar microscope setup was used in Stricker et al. (2008), but to maintain temperature at 37°C a plexiglass incubation temperature was used. At 60x, fluorescent images were taken every 3-4.5 minutes which we found to be sufficient to prevent photobleaching(200-500ms exposure,10% lamp setting). At 20x magnification, fluorescent images could be taken more often (every 2 minutes).

In each device, *E. coli* cells are loaded from the cell port while keeping the media port at sufficiently higher pressure than the waste port below to prevent contamination (Suppl. Fig4). Cells were loaded into the cell traps by manually applying pressure pulses to the lines to induce a momentary flow change. The flow was then reversed and allowed for cells to receive fresh me-

dia with 0.075% Tween20 which prevented cells from adhering to the main channels and waste ports. For the yeast device experiments (Fig3c,d), we loaded *E. coli* cells in the main region by not adding surfactant during the loading process.

We initially built the device in Suppl.Fig 4a to test the synchronized oscillator in three different trap sizes with 1.65μm high trap regions. We found the 1.65μm height allowed for better growth of cells presumably because of the additional flow of media into the interstitial spaces (as compared to 0.9-1.0μm high traps). A parallelized version of the chip with 3 channel heights was constructed to generate different flow rates and trap sizes of (70,84,90,100)x100 μm(Suppl. Fig3b). We found that the heights of the channels did not greatly affect the period measurements presumably since the relevant parameter is only the flow rate in the plane of the trap, and this did not significantly differ between channel heights. Thus, to alter the flow rates we increased the heights of the media reservoir to create different flow rates. To estimate flow rates, we measured the length of traces of fluorescent beads (1.0 μm) upon 100ms exposure to fluorescent light to establish a measure for the average velocity of as a function of height of the media reservoir. We averaged over at least 1000 data points for each to obtain the average velocities in Fig.2c (x-axis), which confirmed that the velocity scales linearly with the pressure difference caused by the height of the media reservoir.

To study spatial temporal behavior of the synchronized oscillator, we designed a microfluidic trap that is 20 times as long (2mm) and 100 μm wide as the original traps (Suppl. Fig4c). Unlike the traps in Suppl. Fig 4*a,b*, the trap is only 0.95 μm high and we found this height optimal for seeding cells in the trap. Since the trap lacks any walls it is open to the flow, it would be difficult to seed cells in a non constraining device. Given the open boundary conditions and the constriction of rod-shaped *E. coli* bacteria to one layer, cells arrange parallel to each other and perpendicular to the edges of the trap. This ordering leads to a very tight packing of a monolayer of cells. Under these conditions, the transport of nutrients, AHL and cell waste happen mainly by diffusion and is less sensitive (but not insensitive) to the flow rate of surrounding media than in the cell traps of devices *a* and *b* below. An example of this is that bursts of fluorescence propagate in both directions of the trap irrespective of the sense of external flow at very high flow rates. In the experiment shown in Suppl. Movie 3, the flow rate was set close to 100 μm/s to counter the increased adherence of cells after long run times, which we believe might be caused by growing them in media with surfactant Tween 20 after long durations.

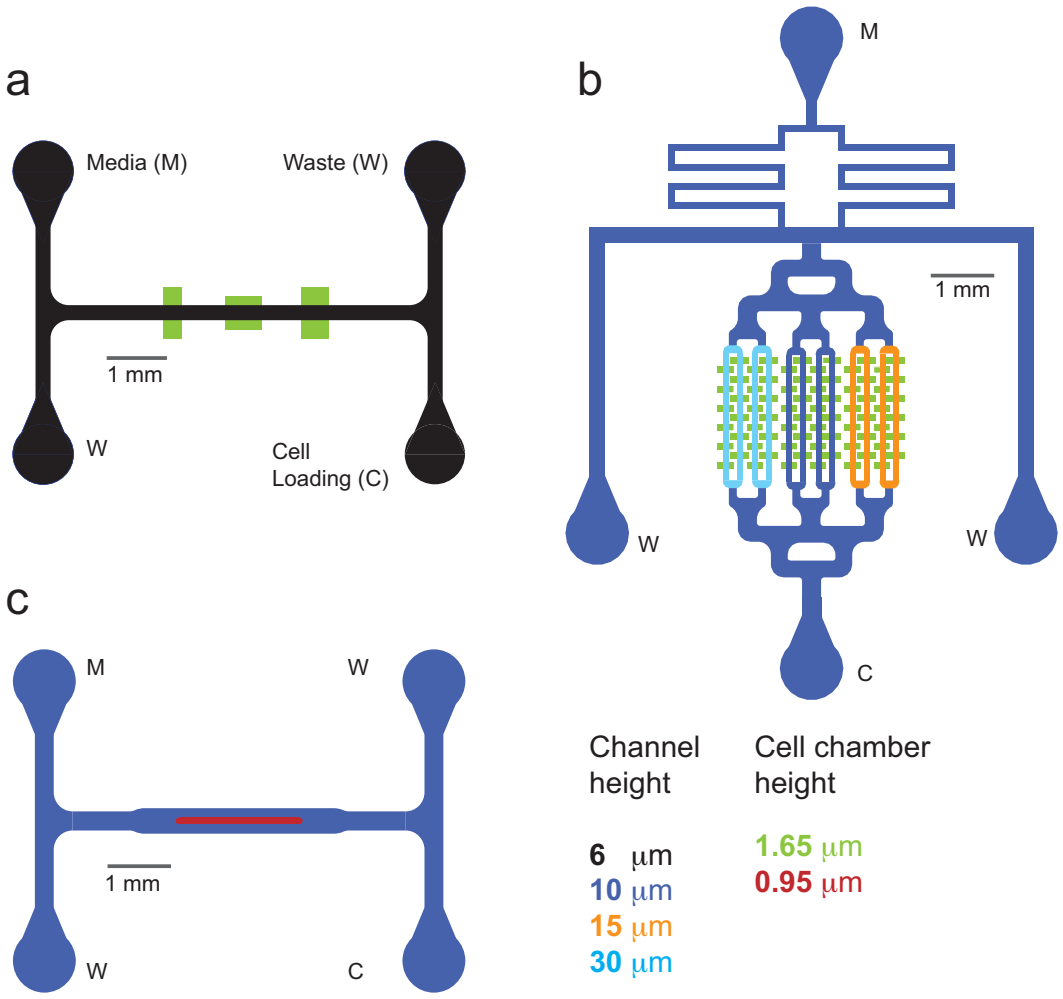

Supplementary Figure 4: Microfluidic Devices constructed for this study. *a)* Device used initially to test the TDSQ1 cells for synchronized oscillations. The dimensions of the traps from left to right are 100x100 μm , 200x50 μm and 150x100 μm, respectively. Traps scaled 300 % in this schematic for visualization. *b)* Parallelized version of Device *a*. Several trap sizes and channel heights could be tested simultaneously. Traps are 100 μm wide and either 70,84,90,or 100 μm deep. *c)* Device used for the wave propagation experiments in Fig3a,b in the main text. The trap is 2000x100 μm wide.

Modeling

There has been much work on modeling asynchronous, oscillating cells coming into synchrony in the context of synthetic biology (McMillen et al. (2002); Garcia-Ojalvo et al. (2004)), though less attention has been focused on gene networks that do not oscillate in individual cells but oscillate collectively (Ma and Yoshikawa (2009)). Here we constructed a deterministic model of quorum-sensing gene clock. From the biochemical reactions depicted in Fig. 1a, we derived the following set of delay-differential equation model for intracellular concentrations of LuxI (I), AiiA (A), internal AHL (H_i), and external AHL (H_e),

$$\frac{\partial A}{\partial t} = C_A[1-(d/d_0)^4]\ P(\alpha,\tau) - \frac{\gamma_A A}{1+f(A+I)} \quad (1)$$

$$\frac{\partial I}{\partial t} = C_I[1-(d/d_0)^4]\ P(\alpha,\tau) - \frac{\gamma_I I}{1+f(A+I)} \quad (2)$$

$$\frac{\partial H_i}{\partial t} = \frac{bI}{1+kI} - \frac{\gamma_H A H_i}{1+gA} + D(H_e - H_i) \quad (3)$$

$$\frac{\partial H_e}{\partial t} = -\frac{d}{1-d}D(H_e - H_i) - \mu H_e + D_1\frac{\partial^2 H_e}{\partial x^2} \quad (4)$$

We did not include an equation for LuxR assuming that it is constitutively produced at a constant level. Previous work found that LuxR is under control of the LuxR-AHL complex to produce a higher concentration of LuxR but we did not find this necessary to capture the essential behavior of the synchronized oscillator(Williams et al. (2008)).

In the first two equations, the Hill function

$$P(\alpha,\tau) = \frac{\delta + \alpha H_\tau^2}{1+k_1 H_\tau^2}$$

describes the delayed production of corresponding proteins, it depends on the past concentration of the internal AHL, $H_\tau(t) = H_i(t-\tau)$. These delayed reactions mimic the complex cascades of processes (transcription, translation, maturation, etc.) leading to formation of functional proteins. The pre-factor $[1-(d/d_0)^4]$ describes slowing down of protein synthesis at high cell density d due to lower nutrient supply and high waste concentration. Terms proportional to γ_x describe enzymatic degradation of proteins and AHL by proteases inside of the cell due to their degradation tags. We model these processes using Michaelis-Menten kinetics. Terms proportional to D describe diffusion of AHL through cell membrane, and the term proportional to μ models dilution of external AHL by external fluid flow. The cell density (d) determines the amount of external AHL and thus affects the AHL decay rate. The factor $d/(1-d)$ follows from the total mass conservation of AHL inside and outside the cells. Since the flow speed ($\sim 100\mu$m/sec) is much higher than the typical wave propagation speed ($\sim 10\mu$m/sec), we neglected the anisotropy imposed by the fluid flow. The last term in equation for H_e describes the diffusion of external AHL.

We used the following experimentally relevant scaled parameters in most of our simulations: $C_A = 1, C_I = 4, \delta = 10^{-3}, \alpha = 2500, \tau = 10, k = 1, k_1 = 0.1, b = 0.06, \gamma_A = 15, \gamma_I =$

24, $\gamma_H = 0.01, f = 0.3, g = 0.01, d_0 = 0.88, D = 2.5$. We varied the diffusion constant D_1 and the external AHL decay rate (flow rate) μ, as well as the cell density d. For "bulk" simulations we dropped the diffusion term $\sim D_1$ in equation for H_e, and solved the resulting set of ordinary delay-differential equations. For spatio-temporal simulations we replaced the partial delay-differential equations by a one-dimensional array of $N = 200$ systems of ordinary delay-differential equations representing individual "cells" coupled via a second-order discrete diffusion operator $D_1 dx^{-2}[H_{i-1} + H_{i+1} - 2H_i]$ for the external AHL concentration. We used periodic boundary conditions at the ends of the array ($H_1 = H_N$).

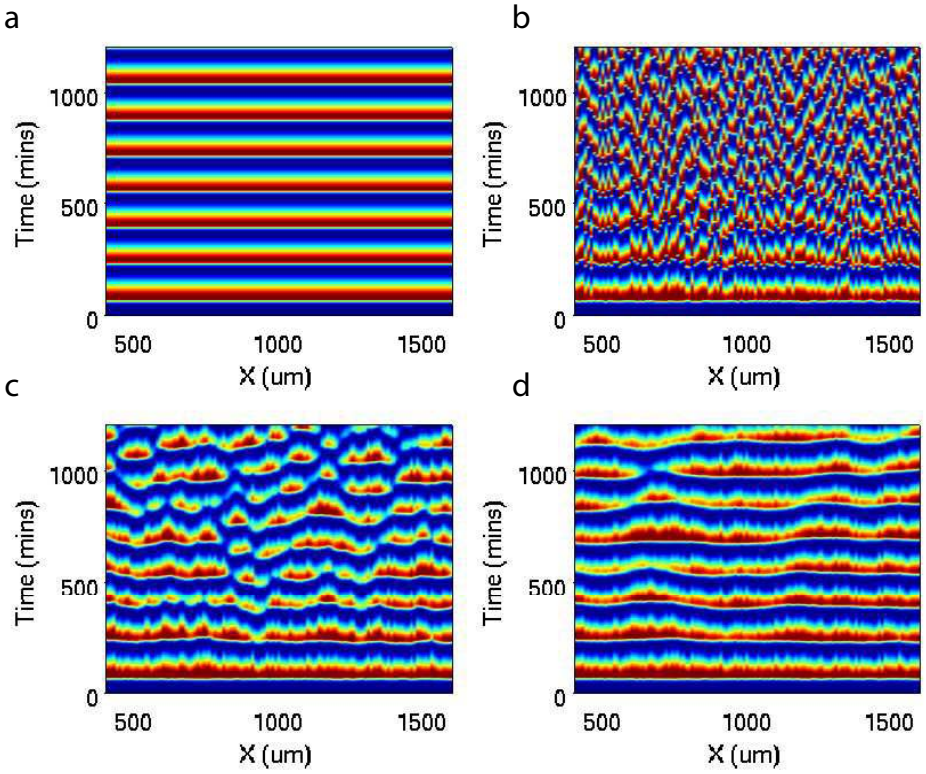

Supplementary Figure 5: Synchronization of oscillations in spatially extended system with diffusion. The parameters (p) of each of 200 oscillators were varied around their nominal values (p_0) as $p = p_0(1 + \eta\xi)$ where ξ is a random number uniformly distributed between -0.5 and 0.5, and η characterizes the fluctuations magnitude. To illustrate the role of spatial diffusion in mitigating the stochastic fluctuations, we varied η and D_1: a, $\eta = 0$, $D_1 = 0$, b, $\eta = 0.1$, $D_1 = 0$, c, $\eta = 0.1$, $D_1 = 800\mu\text{m}^2/\text{sec}$, d, $\eta = 0.1$, $D_1 = 4000\mu\text{m}^2/\text{sec}$,

In addition to the numerical results presented in the Main Text, we show here the results of additional spatiotemporal simulations. In particular, Suppl. Fig. 5 shows the synchronization of oscillations in cell population with statistically different parameters. As seen from the figure, the coherence of oscillations increases with the diffusion coefficient D_1, as expected. In Suppl. Fig. 6 we show the propagation of waves initiated by a localized initial condition ($I_{N/2} = 1$ while all other $I_i = 0$ and $A_i = 0$) for different diffusion constants. Since parameter δ characterizing the leakiness of the *luxI* promoter is small (10^{-3}), the basal state with $A = I = 0$ is very weakly unstable. Thus, in the absence of AHL diffusion ($D_1 = 0$), while the middle cell begins to

oscillate immediately, all other cells are still quiescent (Suppl. Fig. 5a). However, when the diffusion is present ($D_1 \neq 0$), cells influence their neighbours and oscillations propagate in the form of traveling waves in both directions (Suppl. Fig . 6b-d). As seen from this set of space-time diagrams, the wave speed increases with D_1. Fig. 4d of the Main text shows that this dependence is well approximated by the formula $V \approx 0.17 d_1^{1/2} \mu$m/sec.

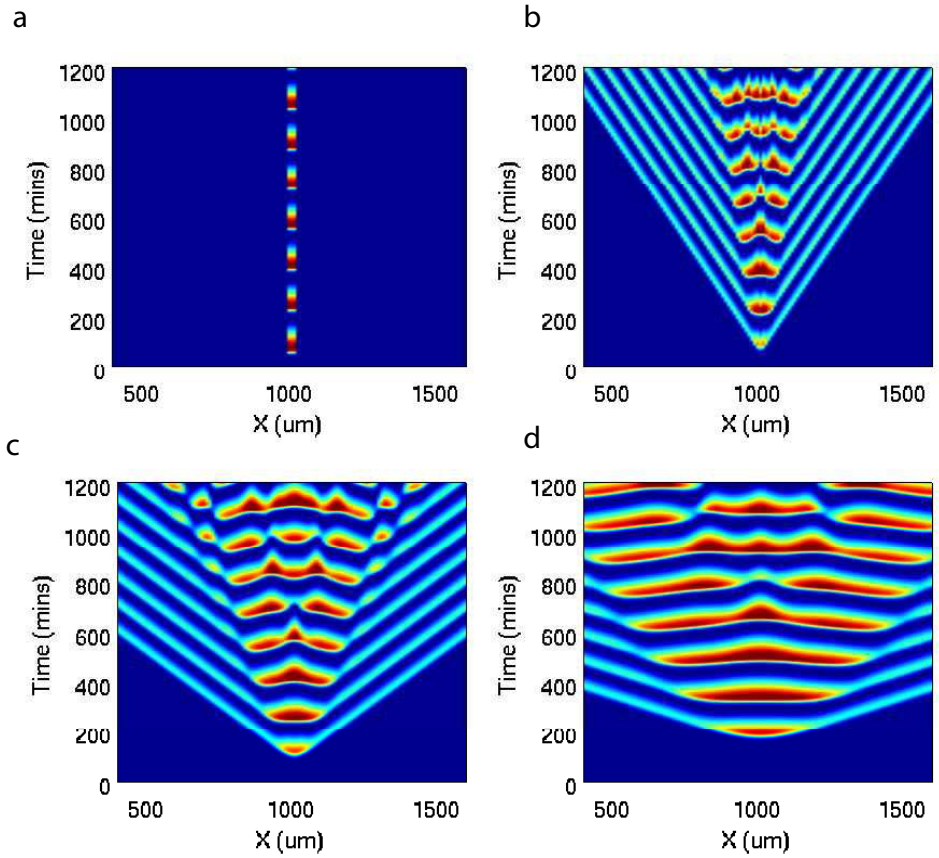

Supplementary Figure 6: Wave propagation in the spatially uniform system with different external AHL diffusion rates: a, $D_1 = 0$, b, $D_1 = 200\mu\text{m}^2/\text{sec}$, c, $D_1 = 800\mu\text{m}^2/\text{sec}$, d, $D_1 = 4000\mu\text{m}^2/\text{sec}$,

References

Dunlap, P. and Greenberg, E. (1985). Control of Vibrio fischeri luminescence gene expression in Escherichia coli by cyclic AMP and cyclic AMP receptor protein. *Journal of bacteriology* 164:45–50.

Garcia-Ojalvo, J., Elowitz, M. and Strogatz, S. (2004). Modeling a synthetic multicellular clock: Repressilators coupled by quorum sensing. *Proceedings of the National Academy of Sciences* 101:10955–10960.

Lutz, R. and Bujard, H. (1997). Independent and tight regulation of transcriptional units in Escherichia coli via the LacR/O, the TetR/O and AraC/I1-I2 regulatory elements. *Nucleic acids research* 25:1203.

Ma, Y. and Yoshikawa, K. (2009). Self-sustained collective oscillation generated in an array of nonoscillatory cells. *Physical Review E* 79:46217.

McMillen, D., Kopell, N., Hasty, J. and Collins, J. (2002). Synchronizing genetic relaxation oscillators by intercell signaling. *Proceedings of the National Academy of Sciences* 99:679–684.

Stricker, J., Cookson, S., Bennett, M., Mather, W., Tsimring, L. and Hasty, J. (2008). A fast, robust and tunable synthetic gene oscillator. *Nature* 456:516–519.

Thomas, P., Stone, E., Costello, A., Tierney, D., Fast, W. et al. (2005). The quorum-quenching lactonase from Bacillus thuringiensis is a metalloprotein. *Biochemistry(Washington)* 44:7559–7569.

Williams, J., Cui, X., Levchenko, A. and Stevens, A. (2008). Robust and sensitive control of a quorum-sensing circuit by two interlocked feedback loops .

Supplementary Movies

Supplementary Movie 1. Timelapse fluorescence microscopy of TDQS1 cells at low flow rate in a 100x100μm trap. Fluorescence is shown in cyan hot color table (dark blue low, white high). Total time of movie is 483 min with a sampling rate of one image every 3 min.

Supplementary Movie 2. Timelapse microscopy of TDQS1 cells at high flow rate in a 100x100μm trap. Fluorescence is shown in cyan hot color table (dark blue low, white high). Total time of movie is 867 min with a sampling rate of one image every 3 min.

Supplementary Movie 3. Timelapse fluorescence microscopy of TDQS1 cells in a 2000x100x0.95μm open trap showing propagation of AHL at millimeter scale. The brightfield image is shown in gray, and fluorescence is shown in cyan hot color table (dark blue low, white high). Total time of movie is 962 min with a sampling rate of one image every 3 min.

Supplementary Movie 4. Zoomed timelapse fluorescence microscopy of TDQS1 cells in a 2000x100x0.95μm open trap showing close-up of cells and propagation of AHL. The brightfield image is shown in gray, and fluorescence is shown in cyan hot color table (dark blue low, white high). Total time of movie is 962 min with a sampling rate of one image every 3 min.

Supplementary Movie 5. Timelapse fluorescence microscopy of TDQS1 cells in a three dimensional 1000x400x4.0μm trap. The brightfield image is shown in gray, and fluorescence is shown in cyan hot color table (dark blue low, white high). Total time of movie is 636 min with a sampling rate of one image every 2.25-4 min.

Supplementary Movie 6. Simulation of the wave propagation within a uniform population of cells. The oscillations are initiated by a small perturbation in the middle of the chamber. The space-time diagram corresponding to this simulation is shown in Fig. 4e of the Main text.

Supplementary Movie 7. Simulation of the wave propagation within a growing dense cluster of cells. The oscillations are initiated by a small perturbation in the middle of the initially small cluster. The space-time diagram corresponding to this simulation is shown in Fig. 4f of the Main text.